paper no. J-037

$Revision: 1.4 $

$Date: 2001/09/14 14:10:58 $

Micromagnetic simulation of domain wall pinning in Sm(Co,Fe,Cu,Zr)$_z$ magnets

W. Scholz, J. Fidler, T. Schrefl, D. Suess, and T. Matthias

Institute of Applied and Technical Physics, Vienna University of Technology, Wiedner Hauptstraße 8-10/137, A-1040 Vienna, Austria

Abstract

Domain wall pinning in Sm(Co,Fe,Cu,Zr)$_z$ based magnets was investigated with 3D-micromagnetic simulations. The pinning effect was studied for varying thickness of the intercellular phase at constant cell size. The simulations showed a complete loss of the pinning effect for a very thin and very thick cell boundary phase. In the proper region the pinning field was calculated for varying anisotropy constant.

Keywords: micromagnetism, domain wall pinning, precipitation, magnetocrystalline anisotropy

Corresponding author

Werner Scholz

Vienna University of Technology

Institute of Applied and Technical Physics

Wiedner Hauptstraße 8-10/137

A-1040 Vienna

Austria

tel: +43 1 58801 13729

fax: +43 1 58801 13798

email: werner.scholz@tuwien.ac.at

Samarium-Cobalt type permanent magnets were discovered in the 1960's by Strnat and coworkers [1]. The high magnetic moment of Sm and Co as well as the high magnetocrystalline anisotropy are the reason for the excellent magnetic properties of this material. Furthermore the high Curie temperature of 720 °C for $SmCo_5$ and 820 °C for Sm_2Co_{17} [2] makes it the best material currently available for high temperature magnets.

Transmission electron micrographs of $Sm(Co,Fe,Cu,Zr)_{7.5-8}$ type magnets show the rhombohedral microstructure of these "pinning" controlled magnets [3, 4]. The fine cell morphology with $Sm_2(Co,Fe)_{17}$ type rhombohedral cells with a typical diameter of 200 nm, which are separated by a $Sm(Co,Cu,Zr)_{5-7}$ type boundary phase, is responsible for the magnetic properties. The cellular precipitation structure is formed during the isothermal aging procedure in the production process. Its development is determined by the direction of zero deformation strains due to the lattice misfit between the different phases [5].

Foucault images of Lorentz electron microscopes show that the cellular precipitation structure acts as a pinning site for magnetic domain walls. The difference in composition between the cells and the cell boundary phase gives rise to a difference in the magnetocrystalline anisotropy. As a result it is energetically favorable for a magnetic domain wall to either stay in the cell boundary phase ("attractive domain wall pinning" if the domain wall energy is lower) or just inside the cells ("repulsive domain wall pinning" if the domain wall energy in the cell boundary phase is higher than that in the cells).

A finite element model of the microstructure of $Sm(Co,Fe,Cu,Zr)_z$ has been developed. It consists of $3 \times 3 \times 3$ rhombohedral cells with a spacer

layer for the cell boundary phase in between (see fig. 1). The edge length e and the "corner angle" β of the rhombohedrons as well as the thickness t of the precipitation are variable. The "space diagonal" D, is parallel to the easy axis. The domain wall of the initial magnetization distribution of our simulations lies in the plane, which is indicated by the thick lines.

The influence of the thickness of the cell boundary phase on the domain wall pinning and the pinning field has been studied. We have used $e = 100$ nm and $\beta = 60°$, which gives $D \approx 250$ nm. The thickness has been varied from $t = 2.5$ nm to $t = 40$ nm. The finite element mesh consisted of 12 597 nodes and 65 708 elements. We have used the following material parameters for 300 K [2]: For the cells ("2:17" type) $J_s = 1.32$ T, $A = 14$ pJ/m, $K_1 = 5$ MJ/m^3. For the cell boundary phase ("1:5" type) we have used $J_s = 0.8$ T, $A = 14$ pJ/m, $K_1 = 1.9$ MJ/m^3. The exchange length is 1.7 nm in the cells and 2.7 nm in the cell boundary phase. Thus, the domain wall width is 5.3 nm in the cells and 8.5 nm in the cell boundary phase. The lower anisotropy in the intercellular phase as compared to the cells leads to "attractive pinning", which means, that the domain wall prefers to move into the intercellular phase and stays there pinned [6].

As we are varying the thickness, the ratio of the volume of the cells $V_{2:17}$ to the volume of the cell boundary phase $V_{1:5}$ changes. Thus, the composition and the z-value changes. These data are summarized in table 1, where a volume of $V_e^{2:17} = 0.24853$ nm^3 and $V_e^{1:5} = 0.0859$ nm^3 for the elementary cells of the "2:17-type" cells and the "1:5-type" cell boundary phase, respectively, have been assumed [7]. The z-value is determined by

$$z = \frac{17 \cdot V_{2:17}/V_e^{2:17} + 5 \cdot V_{1:5}/V_e^{1:5}}{2 \cdot V_{2:17}/V_e^{2:17} + 1 \cdot V_{1:5}/V_e^{1:5}} \quad ,$$

where all additives have been neglected.

The demagnetization curves given in figure 2 show, that for a very thin cell boundary phase (2.5 nm, 5 nm) the effect of domain wall pinning vanishes (no plateau in the demagnetization curve), because the domain wall width is larger than the thickness of the cell boundary phase. Due to magnetostatic effects (magnetic surface charges on the surface of the model) and pinning on the computational grid [8] we still need an external field to move the domain wall. For a thickness of 10 and 20 nm we find strong domain wall pinning. When an external field of about 2500 kA/m is applied, the domain wall can overcome the energy barrier and cross the cell boundary phase. For a cell boundary phase with a thickness of more than 4 times the domain wall width, the analysis of the magnetization distribution reveals, that the cell boundary phase reverses starting from the original position of the domain wall. This leads to the second plateau in the demagnetization curve for $t = 40$ nm in figure 2. Only at higher fields the magnetization reversal of the cells starts with the nucleation of a reversed domain in a corner of the rhombohedral cells.

In order to study the influence of the material parameters on the pinning behavior, we have varied the anisotropy constant K_1 of the precipitation between 0.4 MJ/m^3 (to mimic almost isolated cells or a close to paramagnetic - Cu rich - intercellular phase, A and J_s have also been reduced) and the value for the cells. The demagnetization curves in figure 3 have been obtained for cells with $e = 50$ nm and $\beta = 60°$, which gives $D \approx 125$ nm, and $t = 5$ nm. For very low values of the anisotropy constant we find very high pinning fields, because the magnetization reversal mode switches to nu-

cleation. As K_1 approaches the value for the cells (2:17 phase) the pinning effect disappears.

Thus, for constant thickness of the intercellular phase, the pinning field increases with increasing difference in the magnetocrystalline anisotropy ΔK_1 between the cells and the cell boundary phase. For given material parameters the thickness of the intercellular phase must not be smaller than the domain wall width. If it is thicker than approximately 4 times the domain wall width, the intercellular phase reverses completely before the cells reverse their magnetization.

The second possible pinning mechanism is repulsive pinning on a cell boundary phase with higher magnetocrystalline anisotropy.

The demagnetization curves for repulsive pinning and different values of the anisotropy constant of the intercellular phase are shown in figure 4. For only slightly enhanced values of the anisotropy constant K_1 we find no pinning, but for $\Delta K_1 \geq 4.0$ MJ/m^3 the pinning fields exceed 2 kA/m. In this regime the pinning field is directly proportional to ΔK_1.

In order to improve the magnetic properties of pinning controlled Sm(Co,Fe,Cu,Zr)$_z$ magnets the thickness and the composition of the cell boundary phase have to be optimized. As the difference between the anisotropy constants of the cells and the cell boundary phase increases, the pinning field and as a result the coercive field of the magnet increase in the regime of attractive as well as in that of repulsive pinning. However, our simulations show, that the thickness of the cell boundary phase plays a crucial role for attractive domain wall pinning, since it must not be too thin, for the domain wall to "fit in" and it must not be thicker than 4 times the domain

wall width.

This work is supported by the EC project HITEMAG (GRD1-1999-11125).

References

[1] K. J. Strnat, G. Hoffer, J. Oson, W. Ostertag, J. Appl. Phys. 38 (1967) 1001–1002.

[2] K. D. Durst, H. Kronmüller, W. Ervens, Phys. Stat. Sol. 108 (1) (1988) 403–416.

[3] H. Zijlstra, Permanent magnets; theory, in: H. P. Wohlfarth (Ed.), Handbook on Magnetic Materials, Vol. 3, North-Holland, 1982, Ch. 2, p. 37.

[4] T. Matthias, J. Fidler, G. Zehetner, T. Schrefl, D. Schobinger, G. Martinek, J. Magn. Magn. Mater. Submitted - JEMS'01 paper no. J-034.

[5] J. D. Livingston, D. L. Martin, J. Appl. Phys. 48 (1977) 1350–1354.

[6] H. Kronmüller, Nucleation and propagation of reversed domain in RE-Co-magnets, in: J. Fidler (Ed.), Proceedings of the 6th International Workshop on Rare Eart-Cobalt Permanent Magnets and Their Applications, Tech. Univ. Vienna, Vienna, Austria, 1985, pp. 555–565.

[7] E. Estevez-Rams, TEM study of the correlation between microstructure and magnetic properties of novel hard and soft magnetic materials, Dissertation, TU Vienna (1996).

[8] M. J. Donahue, R. D. McMichael, Physica B 233 (1997) 272–278.

Table and figure captions

Table 1: z-values for different thickness t of the cell boundary phase.

Fig. 1: Geometry of the finite element model.

Fig. 2: Demagnetization curves for varying thickness t (values in the legend in nm) of the intercellular phase.

Fig. 3: Demagnetization curves for varying anisotropy constant K_1 of the cell boundary phase (values in the legend in $\mathrm{MJ/m^3}$) - attractive pinning.

Fig. 4: Demagnetization curves for varying anisotropy constant K_1 of the cell boundary phase (values in the legend in $\mathrm{MJ/m^3}$) - repulsive pinning.

Fig. 5: Pinning field vs. difference in anisotropy constant between the cells and the cell boundary phase.

t (nm)	$V_{2:17}$ (nm^3)	$V_{1:5}$ (nm^3)	ratio	z
2.5	28 738	2 358	12.187	8.13
5	28 738	4 843	5.934	7.81
10	28 738	10 202	2.817	7.31
20	28 738	22 570	1.273	6.64
40	28 738	54 643	0.526	5.93

Table 1: Scholz, paper no. J037

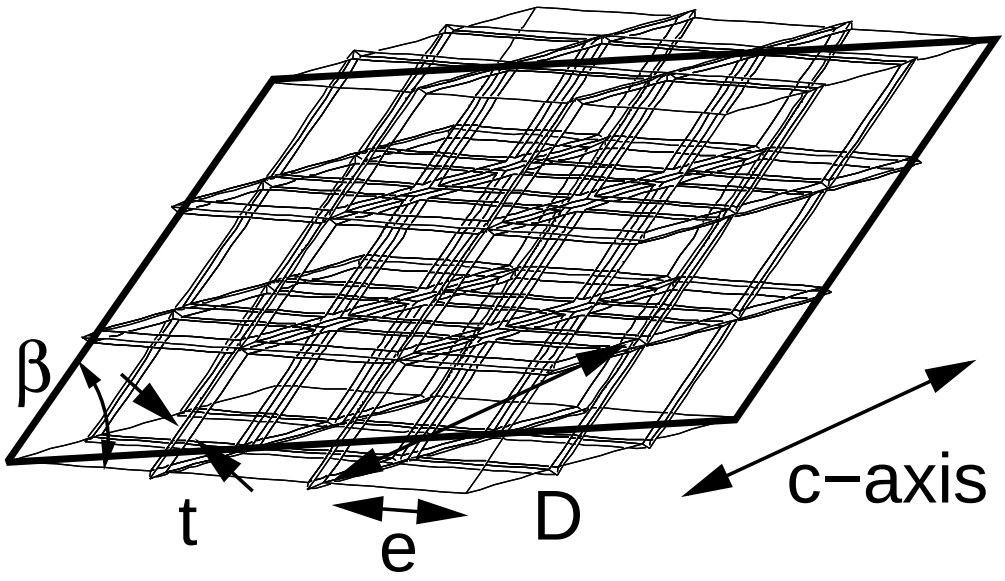

Figure 1: Scholz, paper no. J037

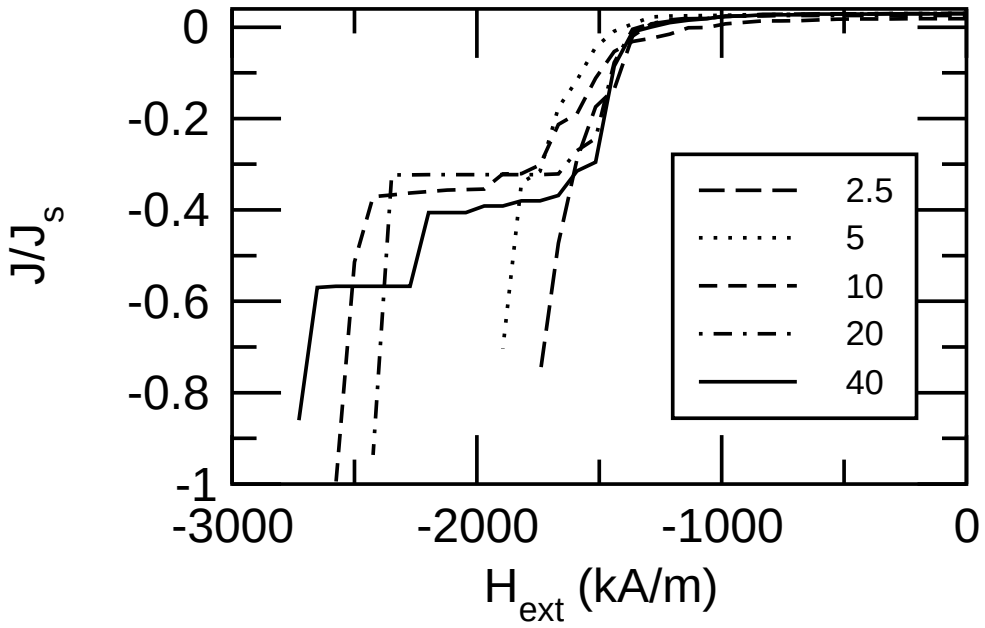

Figure 2: Scholz, paper no. J037

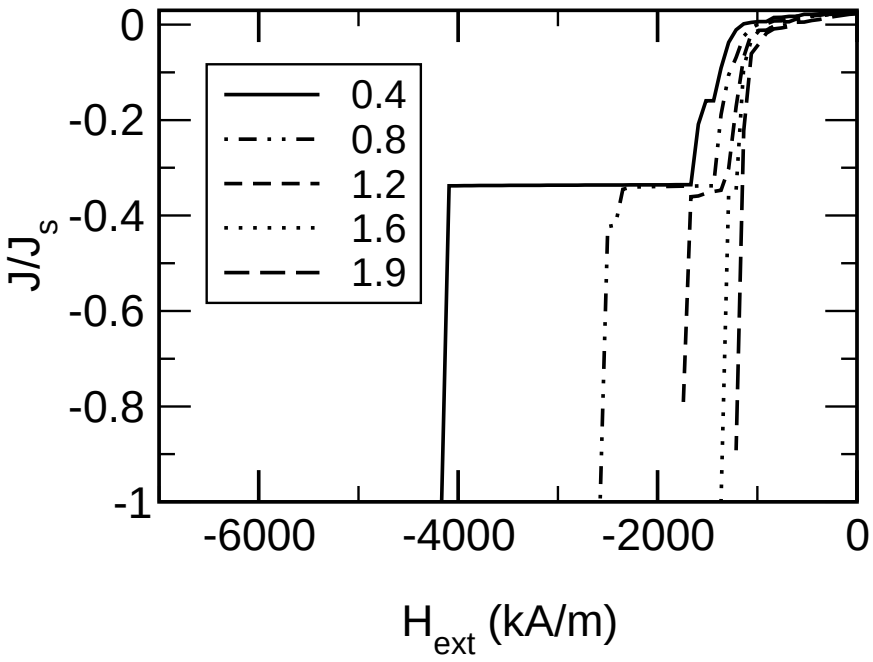

Figure 3: Scholz, paper no. J037

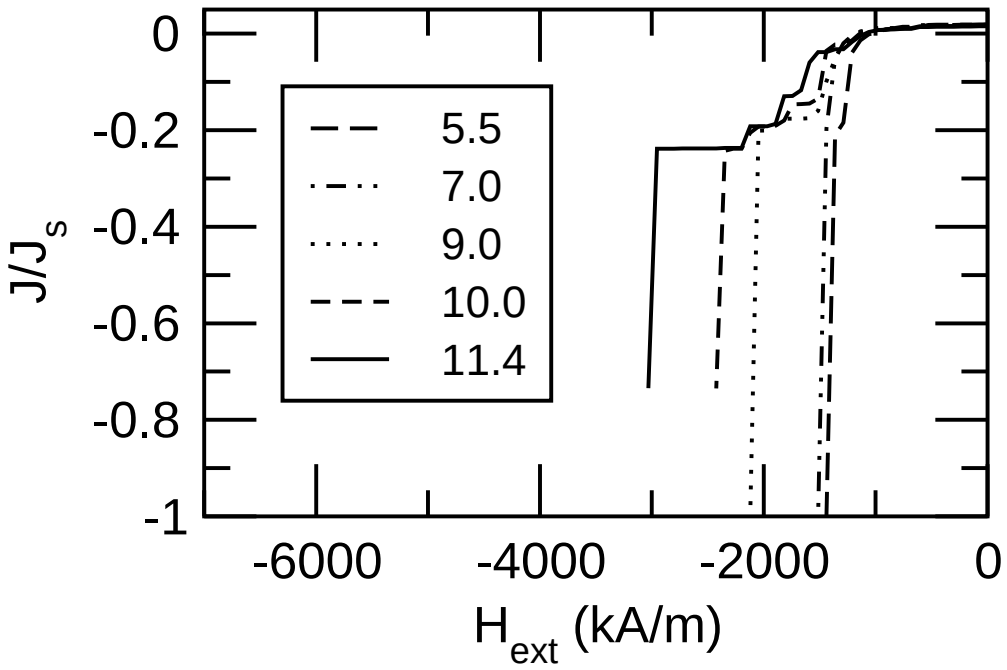

Figure 4: Scholz, paper no. J037

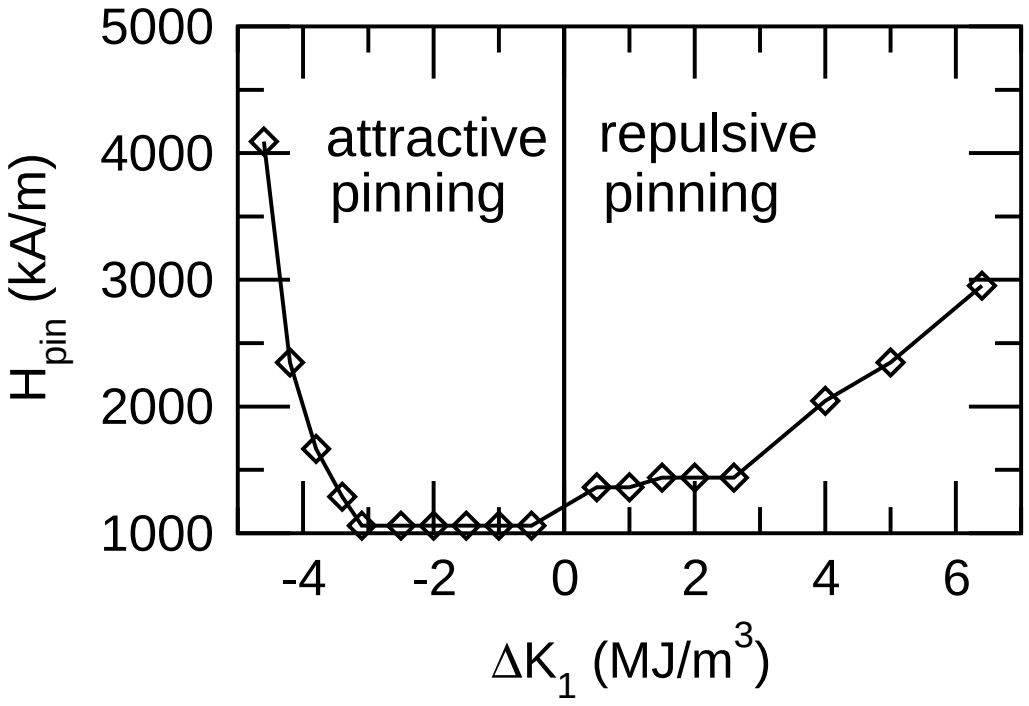

Figure 5: Scholz, paper no. J037